International Journal of Applied Engineering Research ISSN 0973-4562 Volume 10, Number 18 (2015) pp 38714-38719
 https://dx.doi.org/10.37622/IJAER/10.18.2015.38714-38719

1D and quasi-2D numerical models of the cathode temperature in steady-state magnetoplasmadynamic thrusters

Thada Suksila
Department of Mechanical and Aerospace Engineering, Faculty of Engineering,
King Mongkut's University of Technology North Bangkok, 1518 Pracharat Sai I Rd., Wongsawang, Bangsue,
Bangkok 10800, Thailand Phone: +66 096-842-2599, Fax: +66 02-586-9541

Abstract
Electrical thrusters have been developed for increased fuel efficiency of space flight compared to chemical thrusters. Chemical thrusters are limited by the chemical reaction energy in the propellants, whereas electrical thrusters have their own power supply unit to directly input energy into the propellant (i.e., a noble gas). Thus, they have better fuel efficiency. One type of electrical thruster that has potential for future interplanetary journeys is the magnetoplasmadynamic (MPD) thruster. However, the cathode–plasma interaction inside an MPD thruster is not fully understood owing to its complexity and nonlinearity. The objectives of this work were to improve on previous models and explain the interaction between the cathode and nearby plasma region (i.e., sheath) of an MPD thruster in the steady state. Numerical 1D and quasi-2D models were developed by using the explicit method to predict the cathode temperature profile in an MPD thruster. The numerical results were compared with experimental data for verification. The 1D and quasi-2D numerical models partially provide fundamental knowledge on the cathode–plasma interaction and can be used to predict the cathode temperature profile inside an MPD thruster for future design and development

Keywords:Magnetoplasmadynamic (MPD), cathode temperature, cathode numerical models, 1D, quasi-2D

1. Introduction

The magnetoplasmadynamic (MPD) thruster is an electric thruster that uses the Lorentz force created by interaction between the electromagnetic field surrounding the cathode and electrical current field lines passing from the anode to the cathode when it is connected to a high-voltage and high-current power supply. A noble gas (e.g., argon) is injected around the base of the cathode through the crossing electrical current field lines. This heats the argon gas, which is ionized and accelerated through the converging/diverging nozzle, as shown in Fig. 1.

For deep-space maneuvers, the MPD thruster has an advantage over conventional chemical thrusters because it provides a higher specific impulse (I_{sp}), allows for faster maneuvers, and provides approximately twelve times the maneuvers for the same fuel mass [1–3]. The specific impulse I_{sp} of a conventional chemical thruster is approximately 300–500 s; however, an MPD thruster provides a greater I_{sp} of around 2000–7000 s [2, 3]. As a result, MPD thrusters can significantly reduce the mass of a spacecraft at launch. Thus, they are a primary candidate for unmanned and manned travel and cargo spacecraft on interplanetary missions [1–4].

MPD thrusters can typically be categorized as pulsed, steady-state, self-field, or applied-field. This study considered the steady-state and self-field MPD thrusters. The MPD thruster life is known to currently be limited by cathode erosion, which can occur owing to the interaction between the cathode and the plasma region inside the thrusters, especially the plasma sheath. That is, heat transfer in the plasma sheath region can be in either direction depending on the operating characteristics [2–4]. Hence, many numerical models have been developed to predict the cathode temperature profile in an MPD thruster before its malfunction [1, 2, 4, 6].

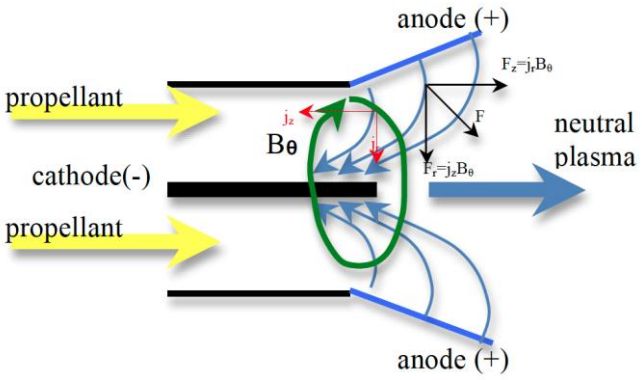

Fig. 1. Diagram of the Lorentz force created in an MPD thruster.

Many experiments have shown that the steady-state temperature of an MPD thruster is about 3000–3500 K at the cathode tip and 500–1500 K at the cathode base depending on the experimental setup [1, 2, 4]. Some numerical models have been developed of the cathode in MPD thrusters that include the transient condition until the system reaches a steady-state condition, and they have confirmed that the cathode tip temperature is around 3000–3500 K [2–4]. The cathode voltage drop, which consumes a great deal of power, has similarly been shown in experiments and numerical models to have an approximate value of -6 to -9 V [2-4].

This paper presents an improvement of the numerical 1D MPD thruster model in [3]. By using the heat diffusion equation with the first-order forward-in-time explicit method, 1D and quasi-2D numerical models can be used to calculate the cathode temperature profile of an MPD thruster in the steady state. That is, the quasi-2D numerical model adds convection or radiation terms to the heat diffusion equation.

International Journal of Applied Engineering Research ISSN 0973-4562 Volume 10, Number 18 (2015) pp 38714-38719
 https://dx.doi.org/10.37622/IJAER/10.18.2015.38714-38719

Both models were compared with experimental data from [1, 2]; the findings are detailed in the following sections.

2. Numerical Model Procedures

For both 1D and quasi-2D MPD thruster numerical models, the plasma and cathode regions are separated by the plasma sheath, which is assumed to have infinitesimal thickness as shown in Fig. 2. Here, the plasma sheath voltage was assumed to be -8.71 V. The plasma sheath properties were as follows: a pressure of 66 Pa, Richardson coefficient of 60 A/(cm^{2}K^2), and work function of 4.5 eV. The total current was varied among 60, 600, 1000, and 1400 A.

The total current was assumed to be constant along the cathode as it accumulated at the tip of the cathode. The cathode tip and base were assumed to achieve a steady-state condition. That is, the temperatures at the cathode tip and base were set to a constant 3300–3500 K and 1500 K, respectively [1–4].

2.1 1D MPD thruster

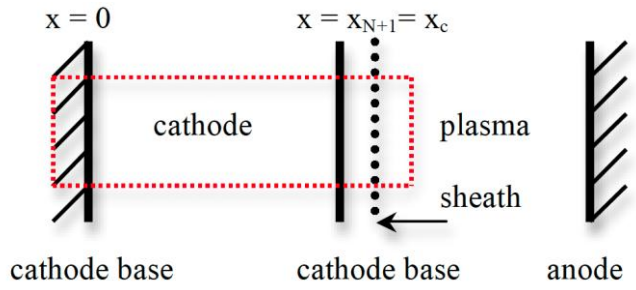

Fig. 2. 1D numerical model of MPD thruster in red region.

2.1.1Grid discretization

The length of each cell L_i can be calculated by using the total length of the cathode region L_{cathode} divided by the total number of cells N. At the cathode base and tip, this can be represented as 0 to x_c. The grid is composed of $N + 1$ points numbered from cells 0 to N. Point 0 is the cathode base, and point $N + 1$ is at the cathode tip, as shown in Fig. 3. Grid point i is located at $x = x_i$. Thus, $x_0 = 0$ and $x_{N+1} = x_c$. Two kinds of cells are defined. Primary cells span the intervals between grid points. There are N primary cells numbered from 1 to N. Primary cell 1 covers the interval between points 0 and 1; more generally, primary cell i covers the interval between point i - 1 and point i. The width of the primary cell L_i is given by

$$L_i = x_i - x_{i-1}. \tag{1}$$

Secondary cells span the intervals between the midpoints of primary cells. There are $N + 1$ secondary cells numbered from 0 to N. The secondary cell i surrounds grid point i. Note that, if the primary cells adjacent to grid point i are of different widths, then grid point i is not the midpoint of secondary cell i. The width of the secondary cell $L_{s,i}$ is given by

$$L_{s,i} = (L_i + L_{i+1})/2 \tag{2}$$

The two secondary cells at the cathode tip and base are bounded by the grid endpoints. Thus, secondary cell 0 ranges from $x = 0$ to $x = L_1/2 = x_1/2$, and secondary cell N ranges from $x = (x_{N-1} + x_N)/2$ to $x_N = x_c$, as shown in Fig. 4. In the primary cells, the thermal conductivity value is taken at the grid points. However, the electrical and thermal conductivities are taken from the cells. The cathode model is based on the properties of tungsten.

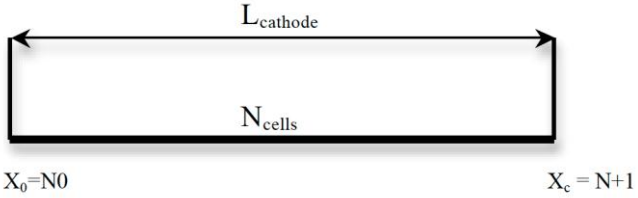

Fig. 3. Cathode region, grids, and cells.

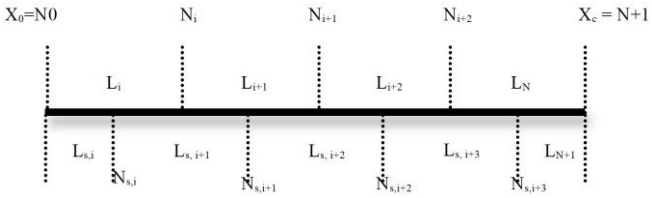

Fig. 4. Grid points in plasma and cathode regions.

2.1.2Equations to be solved

The electric potential ϕ and temperature T are the primary values to be calculated in the models.

Electrical potential:

The external high-voltage and high-current power supply pumps the current density J through the system from the anode to the cathode. Because the system is 1D, the current density is constant throughout the system. In this work, the electrical potential ϕ was -8.71 V at the cathode tip and less than -8.71 V at the cathode base. The electric field can be calculated from

$$E = -\frac{df}{dx}. \tag{3}$$

The temperature values are defined at the grid points; however, the electric field values are defined in the primary cells and can be expressed as

$$E_i = \frac{f_{i-1} - f_i}{L_i}. \tag{4}$$

The current density is defined as

$$J = \sigma_{cond} E. \tag{5}$$

where σ_{cond} is the electrical conductivity. The electric field and current density are negative because the field points from right to left.

Temperature:
In order to calculate the cathode temperature, the one-dimensional thermal diffusion equation is used:

$$c_p \frac{dT}{dt} = \frac{d}{dx}\left(K \frac{dT}{dx}\right) + JE, \quad (6)$$

where C_p, K, t, and x are the heat capacity, thermal conductivity, and time and spatial grids, respectively. Eq. (6) can be discretized as given in [3], and the grid starts from 0 to N:

$$\frac{dT_i}{dt} = \frac{1}{c_p(T_i)}\left[J\frac{f_{i+1} - f_{i-1}}{2} + K(\bar{T}_{i+1})\frac{T_{i+1} - T_i}{L_{i+1}} - K(\bar{T}_i)\frac{T_i - T_{i-1}}{L_i}\right] \quad (7)$$

$$\bar{T}_i = (T_{i-1} + T_i)/2. \quad (8)$$

By using the forward difference and first derivative in time, which has the first-order approximation $O(\Delta t)$, the left-hand side of Eq. (7) can be expressed as

$$\frac{dT_i}{dt} = \frac{T_i^{n+1} - T_i^n}{\Delta t}, \quad (9)$$

where Δt represents the time step and the superscript n represents the number of the time step. This can be rearranged to

$$T_i^{n+1} = T_i^n + \frac{\Delta t}{c_p(T_i)}\left(A + B + C\right). \quad (10)$$

$$A = J\frac{f_{i+1}^n - f_{i-1}^n}{2}. \quad (11)$$

$$B = K(\bar{T}_{i+1}^n)\frac{T_{i+1}^n - T_i^n}{L_{i+1}}. \quad (12)$$

$$C = -K(\bar{T}_i^n)\frac{T_i^n - T_{i-1}^n}{L_i}. \quad (13)$$

The potential is given by

$$f_{i-1}^{n+1} = f_i^n - \frac{JL_i}{\sigma_{cond}(\bar{T}_i^n)}. \quad (14)$$

2.2 Quasi-2D MPD thrusters

The quasi-2D numerical model includes convection and radiation heat transfer at the cathode surface, as shown in Fig. 5.

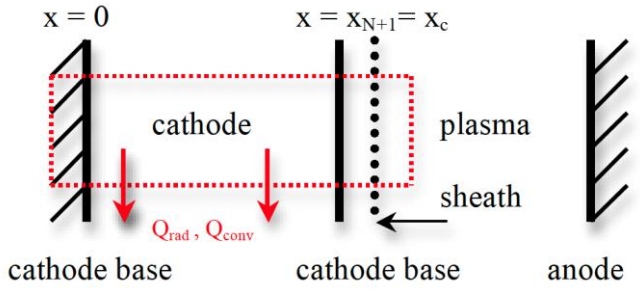

Fig. 5. Quasi-2D numerical model of MPD thruster in red region with radiation and convection.

$$T_i^{n+1} = T_i^n + \frac{\Delta t}{c_p(T_i^n)L_{s,i}}\left(A + B + C - Q_{rad}\right). \quad (15)$$

$$T_i^{n+1} = T_i^n + \frac{\Delta t}{c_p(T_i^n)L_{s,i}}\left(A + B + C - Q_{conv}\right). \quad (16)$$

$$T_i^{n+1} = T_i^n + \frac{\Delta t}{c_p(T_i^n)L_{s,i}}\left(A + B + C - Q_{rad} - Q_{conv}\right). \quad (17)$$

$$Q_{rad} = \sigma_{rad}\varepsilon(T_i^4 - T_{inf}^4). \quad (18)$$

$$Q_{conv} = h_c(T_i - T_{inf}). \quad (19)$$

where h_c, σ_{rad}, ε, T_{inf} are the convective coefficient, Stefan's constant, emissivity, and ambient temperature.

Criteria of the numerical models: The above equations show that the Von Neumann criterion comprises the heat capacity and second-order of the cell length in the numerator and the thermal conductivity term in the denominator. However, the Ohmic heating criterion relates the first order of the cell length and the current density term in the denominator. Both criteria can be expressed as follows:

Von Neumann criterion

$$\Delta t \le \frac{c_p(T_i^n)L_{s,i}L_i}{2K(\bar{T}_{i+1})^n} \quad (20)$$

Ohmic heating criterion

$$\Delta t \le \frac{c_p(T_i^n)L_{s,i}}{J} \quad (21)$$

For this explicit method of the 1D and quasi-2D MPD thruster models, the Von Neumann and Ohmic heating criteria are required to achieve stable and accurate results. That is, the time step should be less than or equal to both criteria.

3. Outline of algorithms

The program is described as follows:

1. Specify the total current I_{total} and radius of the cathode to calculate the cross-sectional area A_c of the cathode. Then, the current density can be calculated as I_{total}/A_c.
2. Create the cells and grid points as explained by Eqs. (1) and (2).
3. Fix the temperature at the cathode base and tip to 1500 and 3,300–3500 K, respectively, and the cathode tip voltage to -8.71 V.
4. Set the initial temperature at each grid point, and calculate the initial electrical conductivity and thermal conductivity values for each primary cell.
5. Calculate the temperature and voltage by using Eqs. (10) and (14) until the temperature adjacent to the cathode base is within 1% of the cathode base temperature. Then, the program will be terminated.
6. For the quasi-2D model, the algorithms and procedures are similar to those of the 1D model; however, the convection and radiation terms are added to the equations, as given in Eqs. (15)–(17). The potential can also be used, as given in Eq. (14).

4. Numerical Results

Fig. 6 shows the trend of the temperature over time at 1, 1.5, and 2 s. Fig. 7 shows that the cathode temperature slightly decreased as the current was increased. The time for the numerical cathode model to reach a steady state is given by t_{ss}. Fig. 8 shows that the cathode temperature was reduced slightly for different cathode diameters. That is, the radial direction of the cathode temperature in the models can be assumed to be constant. The voltage in the cathode increased to lower negative values as the current was increased from 500 A at -8.67 V to 2000 A at -8.55 V, as shown in Fig. 9. However, as the cathode diameter increased, the cathode voltage remained almost constant to the value at a diameter of 30 mm. This was due to the resistivity of the cathode, which linearly decreased with the cross-sectional area as shown in Fig. 10.

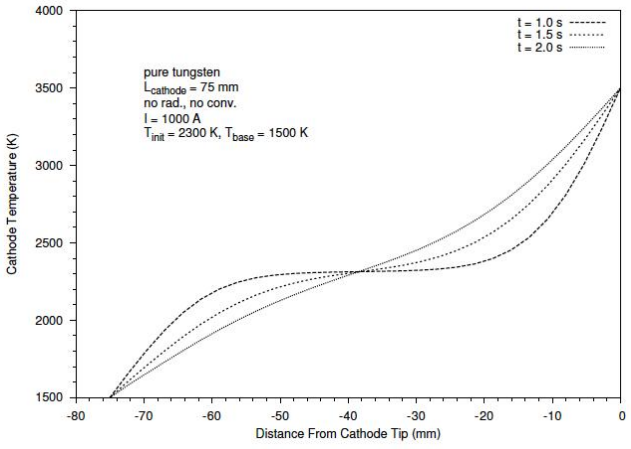

Fig. 6. Cathode temperature as a function of the position from the cathode tip with time as a parameter.

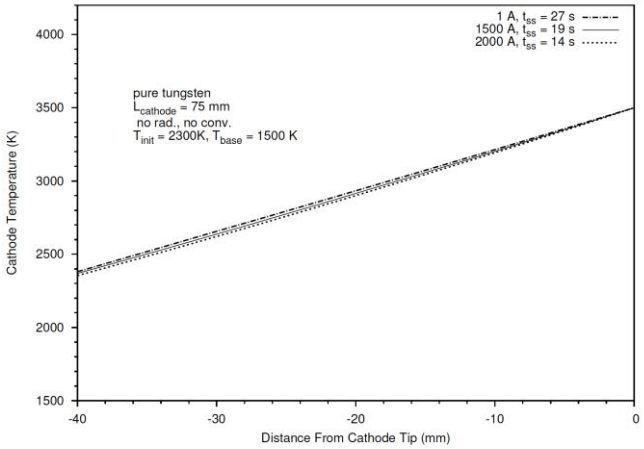

Fig. 7. Cathode temperature as a function of the position from the cathode tip with the current as a parameter.

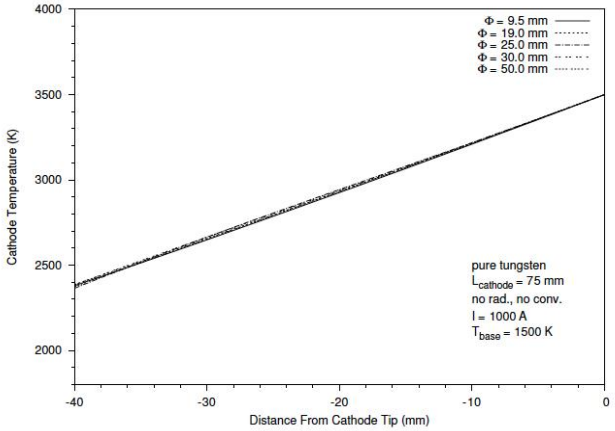

Fig. 8. Cathode temperature as a function of the position from the cathode tip with the diameter as a parameter.

The quasi-2D numerical model of the MPD thruster included and compared the effects of convection and radiation, as shown in Fig. 11. The convection reduced the cathode temperature at the middle of the cathode as the heat was removed to the environment. When radiation was included in the model, the cathode temperature at the middle decreased rapidly. When the convection and radiation were both included, the trend for the temperature was the same as the case considering only radiation. In this study, the case considering convection only was compared with the experimental data.

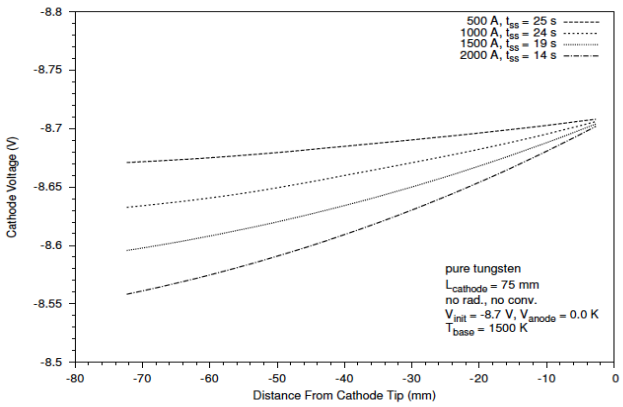

Fig. 9. Cathode voltage as a function of the position from the cathode tip with the current as a parameter.

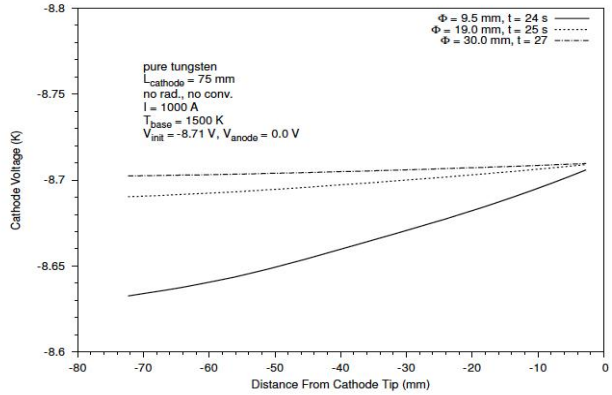

Fig. 10. Cathode voltage as a function of the position from the cathode tip with the diameter (Φ) as a parameter.

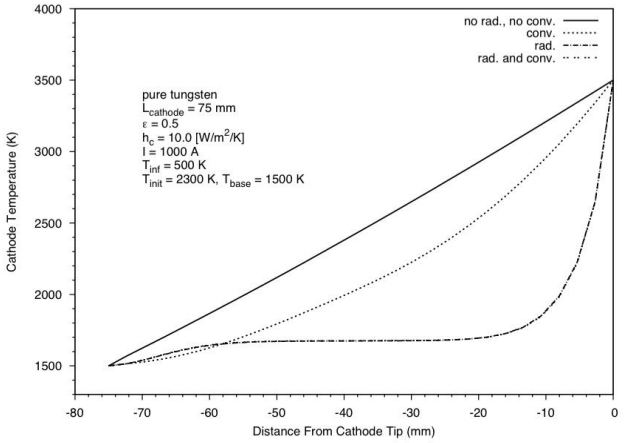

Fig. 11. Cathode temperature considering convection and radiation.

5. Comparison of Models with Experimental Data

In the experiment, the cathode length was 75 mm and the diameter was 3.96 mm. The 1D and quasi-2D numerical models were compared with data from two different experiments [1-2], as shown in Figs. 12 and 13. The experimental data considered currents of 600, 1000, and 1400 A. The 1D numerical model cathode temperature using 1000 A agreed well with the experimental data at 1400 A. For the quasi-2D numerical model, the total current did not significantly change with the cathode temperature, as shown in Fig. 7. However, the changes with convective coefficients of 10, 20, 40 W/m^2/K closely matched the cathode temperature in the experimental results. That is, the results with the convective coefficient at 10 W/m^2/K matched those at 1000 A, and the results around 20 W/m^2/K agreed with those at 600 A.

Thus, the convective heat transfer at the cathode surface must be related to the total current of the system; total currents of 1400, 1000, and 600 A matched convective coefficients of 0, 10, 20 W/m^2/K, respectively. That is, the conductivity heat transfer plays a major role where the total current is above 1400 A as the Ohmic heating generates the heat inside the cathode much greater than the heat convection at the cathode surface. However, the comparison with [1] was not successful because the experimental data had two variables: mass flow (sccm) and pressure (kPa), as shown in Fig. 13. However, the trend smoothly matched the cathode numerical models. Hence, increasing the heat transport coefficient tended to lower the cathode temperature. That is, more heat could be removed from the cathode surface.

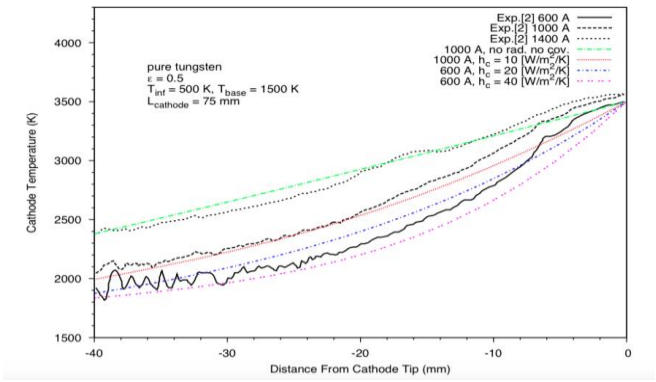

Fig. 12. Comparison between experimental data [2] and numerical results for cathode temperature as a function of the position from the cathode tip.

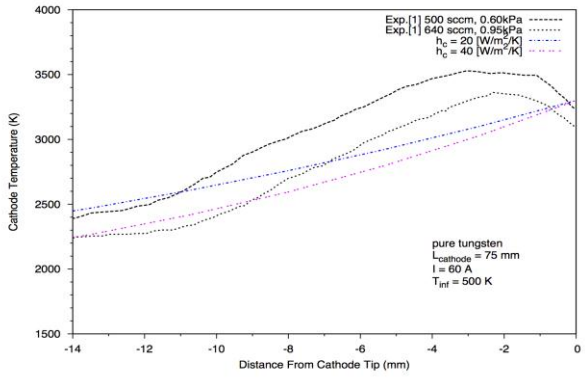

Fig. 13. Comparison between the experimental data [1] and numerical results of the cathode temperature as a function of the position from the cathode tip.

6. Concluding Remarks

This work primarily involved improving the cathode temperature models [3] and explaining the cathode temperature profile for an MPD thruster. These models should help describe experimental phenomena and predict how an MPD thruster will respond to design changes. These models also relate the cathode boundary conditions from a previous model for the steady state of a system where the voltage drop is obtained at the cathode tip [3]. The selected boundary conditions to provide heat to the cathode were consistent with the experimental data—that is, 3500 K and -8.71 V [2] at the cathode tip. Under these conditions, the numerical models were compared with experimental data from several sources [1-2].

The 1D cathode temperature model numerical models agreed well with the experimental data at a total current above 1400 A but were not satisfactory when the current was below 1400 A, as shown in Fig. 12. Thus, the quasi-2D numerical model is preferred because it includes the convection effect, and the cathode temperature agreed quite well at a distance of around -10 mm to the base compared with the experimental results from [1-2]. These discrepancies at the cathode tip to -10 mm had an error less than 1%.

There may be some other effects that have not been included in the 1D and quasi-2D numerical cathode models, such as the electroarc edge [3] where the plasma arc edge is attached to the cathode. Thus, future research will involve completing a 2D cathode temperature numerical model with a magnetic effect where the simulation can be simultaneously compared with experimental data at each time step.

In this study, the objective of predicting the cathode temperature in an MPD thruster was achieved. Because of the present unavailability of experimental cathode temperature data for the MPD thruster above 1400 A, these cathode numerical models may need to be re-checked and compared if the data become available later on.

References

[1] D.A. Codron, D. Erwin, Experimental studies on high current arc discharges for magnetoplasmadynamic thrusters, in: 2012 IEEE Aerospace Conference, Big Sky (MT), 3–10 Mar. 2012, pp. 1–9.

[2] K.D. Goodfellow, A theoretical and experimental investigation of cathode processes in electric thrusters, PhD thesis, University of Southern California, 1996, pp. 261.

[3] T. Suksila, The cathode plasma simulation, PhD thesis, University of Southern California, 2015, pp. 51–80, 110.

[4] A. Kawasaki, K. Kubota, I. Funaki Y. Okuno, Numerical simulation of plasma flow in a self-field MPD thruster coupled with electrode sheath, in: 50th AIAA/ASME/SAE/ASEE Joint Propulsion Conference, Cleveland (OH), 28–30 Jul. 2014, pp. 1–14.

[5] W. F. Ahtye, A Critical Evaluation of Methods for Calculating Transport Coefficients of Partially and Fully Ionized Gases, National Aeronautics and Space Administration, 1965, pp. 70-76.

[6] E. Niewood, M. Martinez-Sanchez, Quasi-one-dimensional numerical simulation of magnetoplasmadynamic thrusters, J. Propuls. Power 8(5) (1992) 1031–1039.

[7] C.K.J. Hulston, P.J. Redlich, W.R. Jackson, M. Marshall, F.P. Larkins, R.C. Mehta, S. Andrews, P.V. Ramachandran, Thermal erosion of magnetoplasmadynamic thruster cathode, Int. J. Heat Mass Transf. 39(8) (1996) 1767–1769.

[8] J. Rossignol, S. Clain, M. Abbaoui, The modeling of the cathode sheath of an electrical arc in vacuum, J. Phys. D: Appl. Phys. 36 (2003) 1495.

[9] R.G. Jahn, W. von Jaskowsky, Physics of Electric Propulsion, Vol. 288. McGraw-Hill, 1968.

[10] R.W. Humble, G.N. Henry, W.J. Larson, U.S. of Defense, U. S. Aeronautics, and S. Administration, Space Propulsion Analysis and Design. McGraw-Hill, 1995.

[11] J.E. Polk, Mechanisms of cathode erosion in plasma thrusters, PhD thesis, Princeton University, 1996.

[12] M.I. Boulos, P. Fauchais, and E. Pfender, Thermal Plasmas: Fundamentals and Applications, Vol. 1. Springer, 1994.

[13] D.A. Erwin, J.A. Kunc, Electron temperature and ionization degree dependence of electron transport coefficients in monatomic gases, Phys. Fluids 28 (1985) 3349.

[14] D.A. Erwin, J.A. Kunc, Scalar DC electrical conductivity of partially ionized gases, Comput. Phys. Commun. 42(1) (1986) 119–125.

[15] S. Paik, E. Pfender, Argon plasma transport properties at reduced pressures, Plasma Chem. Plasma Process. 10(2) (1990) 291–304.

[16] G.J. Dunn, T.W. Eagar, Calculation of electrical and thermal conductivities of metallurgical plasmas, Bull. Weld. Res. Counc. 357 (1990) 1–21.

[17] C.E. Moore, Atomic Energy Levels as Derived from the Analyses of Optical Spectra, Vol. 1–3. US Dept. of Commerce, National Bureau of Standards, 1948.

[18] T.K. Bose, High Temperature Gas Dynamics. Springer, 2004.

[19] J. D. Anderson, Hypersonic and High Temperature Gas Dynamics, McGraw-Hill, New York, 1989.

[20] R. M. Myers, MPD thruster technology, NASA Technical Memorandum 105242 AIAA-91-3568, 1991.